Nat. Hazards Earth Syst. Sci. Discuss., https://doi.org/10.5194/nhess-2017-346
Manuscript under review for journal Nat. Hazards Earth Syst. Sci.
Discussion started: 13 October 2017

Natural Hazards and Earth System Sciences
Discussions

Fire danger rating over Mediterranean Europe based on fire radiative power derived from Meteosat

Miguel M. Pinto[1], Carlos C. DaCamara[1], Isabel F. Trigo[2], Ricardo M. Trigo[1], K. Feridun Turkman[3]

[1]Instituto Dom Luiz (IDL), Faculdade de Ciências, Universidade de Lisboa, Lisbon, 1749-016, Portugal
[2]Instituto Português do Mar e da Atmosfera (IPMA), Lisbon, 1749-077, Portugal
[3]Centro de Estatística e Aplicações da Universidade de Lisboa (CEAUL), Faculdade de Ciências, Universidade de Lisboa, Lisbon, 1749-016, Portugal

Correspondence to: Carlos C. DaCamara (cdcamara@fc.ul.pt)

Abstract. We present a procedure that allows the operational generation of daily forecasts of fire danger over Mediterranean Europe aiming to improve state-of-the art modelling skills for classes of high fire danger. The procedure combines historical information about radiative energy released by fire events with daily meteorological forecasts, as provided by the Satellite Application Facility for Land Surface Analysis (LSA SAF) and the European Centre for Medium-Range Weather Forecasts (ECMWF). Fire danger is estimated based on daily probabilities of exceedance of daily energy released by fires occurring at the pixel level. Daily probability considers meteorological information by means of the Canadian Fire Weather Index (FWI) and is estimated using a Daily Model based on a Generalized Pareto distribution. Five classes of fire danger are then associated to daily probability estimated by the Daily Model. The model is calibrated using seven years of data (2010-2016) and validated against the period of January–August 2017. Results obtained show that about 80 % of events releasing daily energy above 10 000 GJ belong to the "Extreme" class of fire danger, a considerably high fraction that is more than the double of the values obtained when using the currently operational Fire Danger Forecast module of the European Forest Fire Information System (EFFIS) or the Fire Risk Map (FRM) product disseminated by the LSA SAF. Besides assisting in wildfire management, the procedure is expected to help in decision making on prescribed burning within the framework of agricultural and forest management practices.

1 Introduction

Wildfires have been identified as the most important threat to forests in Mediterranean Europe (Requardt et al., 2009) that is regularly affected by large and destructive events. These weather-related hazards represent a serious problem to modern societies, with great negative impacts at social, economic and ecological levels and causing significant human casualties (Amraoui et al., 2015). A striking illustration of the magnitude of the problem is provided by the recent tragic episode of June 17, 2017, that took place in central Portugal at Pedrógão Grande-Góis, with an official death toll of 64 people and by the fire

episodes of the last week of July 2017 near Marseille in southeastern France that led to the evacuation of more than 10 000 people in the French Riviera.

According to the last report issued by the European Commission (San-Miguel-Ayanz et al., 2016), during the period 1980-2015 the five Southern Member States (Portugal, Spain, France, Italy and Greece) were affected by a total of 1 751 067 fires that burned 16 121 036 ha, corresponding to a yearly average of 48 641 fires and a burned area average of 447 807 ha per year. This proneness of Mediterranean Europe to be affected by fire is linked to its climate characterized by rainy and mild winters followed by warm and dry summers (Pyne, 2009). A severe fire season is often triggered by a wetter-than usual winter that increases the amount of biomass, followed by a warmer and drier than average spring that leads to higher levels of vegetation stress (Pereira et al., 2013). Extreme weather conditions in summer (high temperature, strong wind, low fuel moisture and low relative humidity) are a key factor in the ignition and spread of large wildfires (Amraoui et al., 2013; Ruffault et al., 2016).

The role played by meteorological factors in the occurrence of severe fire episodes is conveniently assessed by means of indices of meteorological fire danger that rate the likelihood of a fire event (Finney, 2005). The Fire Weather Index (FWI) that is part of the Canadian Forest Fire Weather Index System (CFFWIS) provides a numeric rating of fire intensity and is particularly suitable as a general index of meteorological fire danger (Van Wagner, 1974; 1987; Stocks, et al., 1989), namely for the ecosystems of Mediterranean Europe (Viegas et al., 1999). Currently FWI is on the basis of the Fire Danger Forecast module of the European Forest Fire Information System (EFFIS) implemented by the European Commission (San-Miguel-Ayanz et al., 2012) as well as of the Fire Risk Map (FRM) product disseminated by the Satellite Application Facility for Land Surface Analysis (LSA SAF) that is part of the EUMETSAT application ground segment (Trigo et al., 2011). However, FWI was specifically designed for the Canadian forest and therefore should be calibrated to the vegetation cover and meteorological conditions over the Mediterranean region (DaCamara et al., 2014).

We present a methodology to assess fire danger based on the estimation of the probability of exceedance of predefined thresholds of daily released energy by active fires as derived from satellite observations of fire radiative power, a physical quantity that is especially useful in fire management and firefighting (Roberts and Wooster, 2008). The procedure is applied to Mediterranean Europe and is calibrated with data covering the period 2010-2016. First, estimates of static probability (i.e. not depending on the day of the year) are obtained, for each location, by dividing the recorded number of fires exceeding a given threshold of energy and observed within a cell centered on each pixel by the total number of fires observed within the same cell. Then it is shown that statistical models based on Generalized Pareto (GP) distributions adequately fit to the upper tails of the observed distributions of released energy and that these models can be improved by integrating both the estimates of static probability and daily FWI as covariates of the scale parameter of the GP distributions. The rationale is that small fires have a weak dependence on daily weather whereas larger fires strongly depend on meteorological conditions (Ruffault et al., 2016). Five classes of fire danger are then attributed to each pixel on a daily basis, taking into account both the values of probability of exceedance and the respective deviations from a long-term mean. Performance of the methodology is assessed by comparing, for different ranges of daily released energy by fires, the distributions of observed events among the five classes of danger with the corresponding distributions when using the classes of fire danger from the above mentioned LSA SAF

Nat. Hazards Earth Syst. Sci. Discuss., https://doi.org/10.5194/nhess-2017-346
Manuscript under review for journal Nat. Hazards Earth Syst. Sci.
Discussion started: 13 October 2017

Natural Hazards and Earth System Sciences Discussions

product and EFFIS module. Finally, the procedure is validated by applying it to the period January–August 2017 and by analyzing the two above mentioned extreme events that took place in Portugal and France, in June and July 2017, respectively.

2 Data

The study area is defined by latitude circles of 35 and 45ºN and meridians of 10ºW and 27.5ºE (Fig. 1) and the study period spans from January 2010 to August 2017. The sub-period from January 2010 to December 2016 is used to calibrate the models whereas the remaining sub-period from January to August 2017 is retained for validating results against independent data. The two sub-periods will be referred hereafter as calibration and validation periods. Both satellite and meteorological data are gridded in the Normalised Geostationary Projection (NGP) of MSG (EUMETSAT, 1999) whose spatial resolution is about 0.04º over the Mediterranean region.

Information about vegetation cover/land use was obtained from the GLC2000 database (Hartley et al., 2006). Originally available at a 1 km resolution, vegetation types were re-projected onto the MSG NGP grid. The 22 types of vegetation/land use were merged into the following 3 main types: 1 to 10 – forest, 11 to 15 – shrubland and 16 to 18 – cultivated areas (Fig. 1).

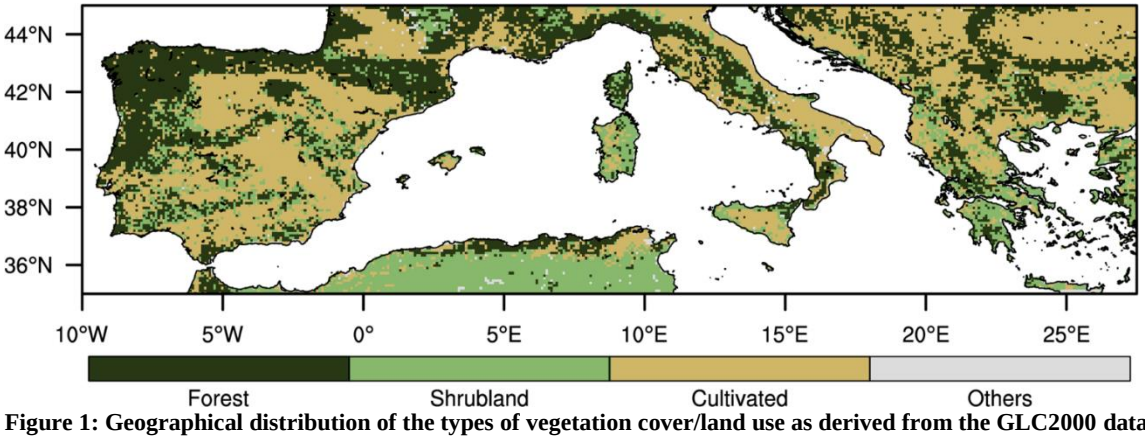

Figure 1: Geographical distribution of the types of vegetation cover/land use as derived from the GLC2000 database.

Data of fire radiative power from January 2010 – August 2017 were obtained from the Fire Radiative Power (FRP) Product generated and disseminated by the LSA SAF (Trigo et al., 2011; Wooster et al., 2015). The FRP product consists of estimates of the radiative power emitted by landscape fires and is derived on a pixel-by-pixel basis from the Spinning Enhanced Visible and Infrared Imager (SEVIRI) instrument, which operates on-board the Meteosat Second Generation (MSG) series of EUMETSAT geostationary satellites (LSA SAF, 2015). The product is provided for the whole MSG disk (up to 72º view zenith angle) every 15-minutes and each active fire location in the study area is represented at the centre of the corresponding SEVIRI pixel. The database provides for each event the geographical coordinates, the date and time, the fire confidence and

Nat. Hazards Earth Syst. Sci. Discuss., https://doi.org/10.5194/nhess-2017-346
Manuscript under review for journal Nat. Hazards Earth Syst. Sci.
Discussion started: 13 October 2017

the fire radiative power (expressed in MW). A full description of the product and its validation is available in the on-line documentation provided at the LSA SAF site (http://lsa-saf.eumetsat.int).

Meteorological data covering the period from January 1979 to December 2016 were obtained from the ERA-Interim reanalysis dataset (Dee et al., 2011) generated by the European Centre for Medium-Range Weather Forecasts (ECMWF). With the aim of recreating the kind of information available when using the developed model in operational mode, data respecting to the validation period (from January to August 2017) consisted of ECMWF's operational 24-hour forecasts (Haiden et al., 2016). Both reanalysed and forecasted data fields consist of daily 12 UTC fields of 24h cumulated precipitation (from 12 UTC of the previous day to 12 UTC of the current day), 2m air temperature and dew point, 10m zonal and meridional wind components. Since the spatial resolution of the reanalysis is about 0.75º, data were re-projected onto the MSG NPP grid. In the case of 2m and dew point temperatures, a topographical correction was performed on the data by applying a constant lapse rate of -0.67ºC/100m to the difference between the surface height of ECMWF model and that of SEVIRI nearest pixels, assuming a constant dew point depression. Relative humidity was computed based on values of temperature and dew point temperature at 2m, according to the Magnus expression (Lawrence, 2005).

3 Methods

3.1 Fire Weather Index

Daily values of FWI covering the period from January 1979 to August 2017 were computed according to the procedure described by Van Wagner and Pickett (1985). For each pixel, the grand average of FWI for all days of the period 1979–2016 hereby denoted $\overline{FWI}$, was also computed. The spatial distribution of $\overline{FWI}$ (Fig. 2) shows a general tendency to decrease with increasing latitude that reflects the same behaviour of the surface temperature field. The spatial distribution is also consistent with the land cover (Fig. 1), the forested areas tending to be associated to lower values $\overline{FWI}$. Other factors such as topography and proximity to the sea are also relevant, the values of $\overline{FWI}$ tending to be lower over the mountains and along the coast. For each pixel p of the MSG NPP grid and for each day d of the study period, the anomaly FWI^*_{pd} was defined as

$$FWI^*_{pd} = FWI_{pd} - \overline{FWI}_{\mathrm{p}}\,, \qquad (1)$$

where FWI_{pd} is the FWI value for pixel p and day d day and $\overline{FWI}_p$ is the grand average of FWI for that pixel. Use of anomalies instead of values of FWI aims at reducing all the above-mentioned factors that regionally affect FWI over Mediterranean Europe as well as mitigating the impacts associated to the delay in solar time (1 hour every 15º towards the east) given that all meteorological fields are defined at 12 UTC (DaCamara et al., 2014).

Nat. Hazards Earth Syst. Sci. Discuss., https://doi.org/10.5194/nhess-2017-346
Manuscript under review for journal Nat. Hazards Earth Syst. Sci.
Discussion started: 13 October 2017

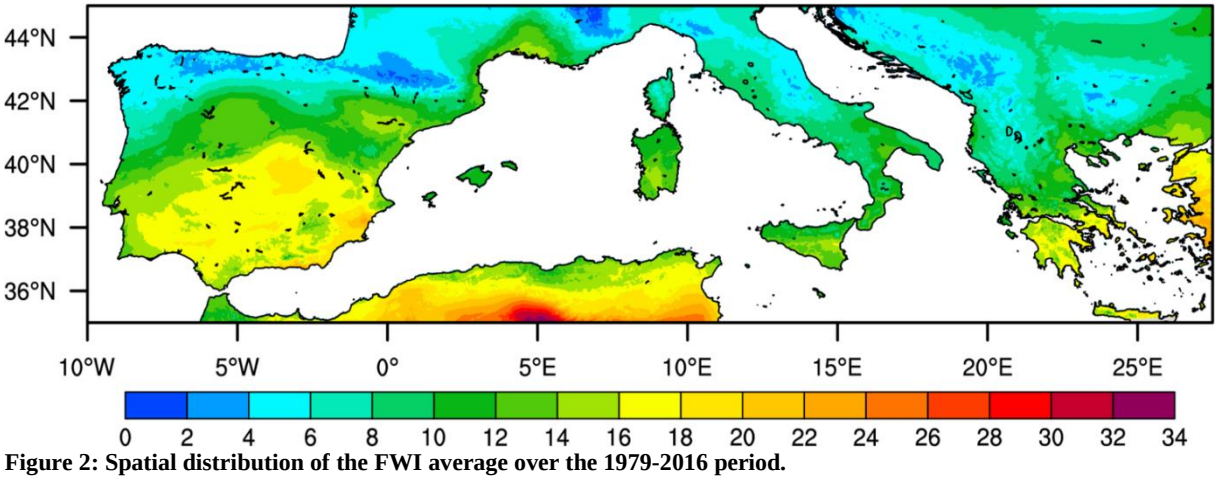

Figure 2: Spatial distribution of the FWI average over the 1979-2016 period.

3.2 Daily energy released by fires

Daily energy released by fire at a given pixel was computed by integrating the radiative power recorded by SEVIRI in that pixel along the considered day. Since the data are sampled every 15 minutes the daily energy, E, in GJ, for each pixel p and day d may be estimated as:

$$E_{pd} = 0.9 \times \left(\sum_{k=1}^{96} FRP_{kp}\right)_d \quad (2)$$

where index k indicates the sequence of 15 minute images for each day, FRP_{kp} is the fire radiative power (in MW) in pixel p of image k and the 0.9 factor converts the result into GJ.

3.3 Static probability of exceedance of energy released by fires

Considering the calibration period (2010–2016), the static probability of exceedance of a given threshold E of daily energy released by fires at each pixel p was estimated by counting the total number of daily fire occurrences in pixels with the same vegetation type as p (Fig. 1) located inside a cell centred in the considered pixel with initial size $\delta = 0.7°$ in latitude and longitude. The size was then successively enlarged by increments of $0.05°$ until the maximum size of $20°$ is attained or the total number of events reaches 200. Denoting by $S_p(\delta, E)$ the total number of daily fires inside cell of size δ centred at p and with released energy exceeding E, the probability of exceedance x is estimated as:

$$P_p(E|0) = \frac{S_p(\delta,E)}{S_p(\delta,0)} \quad (3)$$

where $S_p(\delta, 0)$ is the number of all observed daily fire events (i.e. with energy exceeding zero). As suggested by the notation employed, $P_p(E|0)$ may be viewed as a conditional probability, namely the probability that the daily energy released by fires at pixel p is greater than E provided that an ignition has occurred in that pixel. The rationale for this procedure is that the static probability of exceedance is expected to present smooth spatial variability over pixels with the same vegetation type, while steep changes are to be expected among the different vegetation types.

Nat. Hazards Earth Syst. Sci. Discuss., https://doi.org/10.5194/nhess-2017-346
Manuscript under review for journal Nat. Hazards Earth Syst. Sci.
Discussion started: 13 October 2017

Natural Hazards and Earth System Sciences Discussions

3.4 Statistical models of exceedance of energy released by fires

Following DaCamara et al. (2014), the statistical distribution of daily released energy, E, is modelled using the 'peaks over threshold' (POT) approach (Pickands, 1975).

The POT approach uses the Generalized Pareto (GP) distribution as a model to assign probabilities to the exceedances of E over a predefined threshold, i.e. to values $\Delta E = E - E_{min}$ (with $E > E_{min}$) where E_{min} is a prescribed minimum value (de Zea Bermudez and Kotz, 2010). The GP cumulative distribution function of exceedances ΔE is:

$$G(\Delta E|\alpha,\sigma) = 1 - \left(1 + \frac{\alpha}{\sigma}\Delta E\right)^{-\frac{1}{\alpha}} \quad (4)$$

where α and σ are the shape and scale parameters. Value of minimum threshold E_{min} is obtained by plotting the sample mean of the values exceeding successive thresholds against the respective thresholds, the chosen value being such that the dependence becomes linear for values greater than the chosen one (Coles, 2001). The shape (α) and scale (σ) parameters of the GP distribution are then estimated using the maximum likelihood method (Grimshaw, 1993) and the goodness of fit is finally assessed by means of the A^2 test (Anderson and Darling, 1952), the confidence levels for A^2 being estimated by randomly generating 5,000 data samples from the adjusted GP distribution. Details about the procedure may be found in DaCamara et al. (2014).

The obtained model, hereafter referred to as the null model, may be improved by incorporating daily anomalies, FWI^*, and static probabilities, $P(E|0)$, as covariates of the scale parameter in the GP distribution using a feed forward artificial neural network. The network is trained using the Levenberg-Marquardt algorithm (Hagan and Menhaj, 1994). Daily probabilities are then given by:

$$G(\Delta E|\alpha,\sigma_N) = 1 - \left(1 + \frac{\alpha}{\sigma_N}\Delta E\right)^{-\frac{1}{\alpha}} \quad (5)$$

where $\sigma_N = \sigma_N[FWI^*, P(E|0)]$ is the neural network trained model using FWI^* and $P(E|0)$ as inputs and providing the corresponding scale parameter σ, as output.

Performance of the new alternative model, hereafter referred to as the Daily Model because of its dependence on daily values of FWI^*, is compared against the respective null models by using the standard likelihood ratio test (Neyman and Pearson, 1933) which is based on statistic Λ defined as:

$$\Lambda = 2(\ln L' - \ln L) \quad (6)$$

where L and $L'$are the likelihood functions of the null and the Daily Models, respectively.

3.5 Classes of fire danger

Classes of fire danger are defined, based on values of probability of exceedance and of the respective deviations from the expected value. The rationale is that large fires tend to occur in pixels of high probability of exceedance or of high positive deviation from the expected value for a given day of the year and location. For each pixel p and day d, the probability of exceedance G is evaluated using Eq. (5) and the respective anomaly A is computed by subtracting the average of all values of

Nat. Hazards Earth Syst. Sci. Discuss., https://doi.org/10.5194/nhess-2017-346
Manuscript under review for journal Nat. Hazards Earth Syst. Sci.
Discussion started: 13 October 2017

Natural Hazards and Earth System Sciences Discussions

probability of exceedance for that pixel and day of the year over the period 1979–2016. As shown in Fig. 3, five classes of fire danger (conventionally named "Low", "Moderate", "High", "Very High" and "Extreme") are then defined by setting five partitions in the domain G versus A (delimited by dashed lines) by means of four curves $(\gamma_0, \gamma_1, \gamma_2, \gamma_3)$ defined as follows:

$$\gamma_0\text{: } A \equiv 0\,, 0 \le P \le 1 \quad \text{and} \quad \gamma_i (i = 1,2,3)\text{: } A = e^{\frac{\ln(P_n)}{P_n} P}\,, P_n \le P \le 1 \tag{7}$$

where P_n are break points estimated from fire events according to the following criteria: 1) the first break point is set to 0 so that the "Low" class of fire danger encompasses all cases where the probability of exceedance is below average ($A < 0$); 2) the four breakpoints are equally spaced; and 3) the classes "Very High" and "Extreme" should have about the same number of fire events.

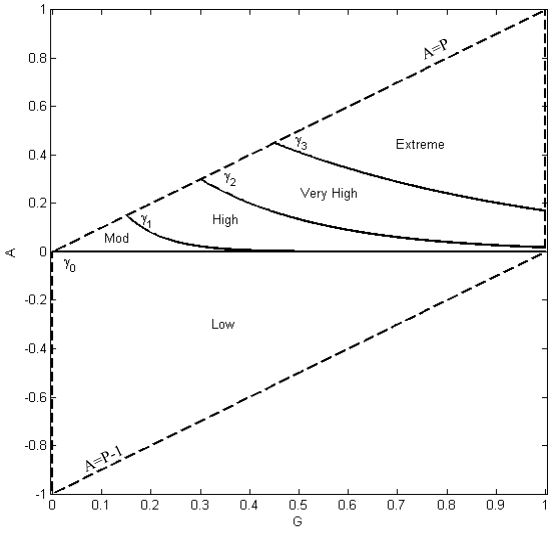

Figure 3: Partitioning of the domain of probability of exceedance, G, versus the respective anomalies, A, into five classes of fire danger named "Low", "Moderate", "High", "Very High" and "Extreme". The partitions are delimited by curves $\gamma_0, \gamma_1, \gamma_2$ and γ_3.

3.6 Model performance and validation

Assessment of performance of the Daily Model is based on a systematic comparison of the distributions of events among classes of fire danger for different ranges of energy released by fire with the corresponding distributions when using classes produced by other products, namely those from EFFIS and the LSA SAF. In the case of EFFIS, six classes are defined by means of a set of breakpoints in FWI that are set up using historical records of large fire events of more than 500 ha of burned area (San-Miguel-Ayanz et al., 2012). The six EFFIS classes are here reduced to five by combining the "Very Low" and the "Low" classes. In the case of the LSA SAF product, the definition of the five classes is based on breakpoints in FWI anomalies that are defined based on information of a probabilistic model of exceedances of active fire duration (DaCamara et al., 2014). Given that classes from the Daily Model are based on probabilistic information about exceedances of energy released by fires,

when comparing against EFFIS and LSA SAF products, the Daily Model is expected to provide a better discrimination of events among classes from the point of view of energy released particularly for the most severe classes.

The validation of the Daily Model is performed for the January–August 2017 (validation) period, by comparing the distributions of daily fire events among classes of fire danger with those obtained for the calibration period (2010 – 2016). Two severe events that took place during the validation period are also examined, namely the fires at Pedrógão Grande-Góis and near Marseille in south-eastern France, which were already mentioned in the introductory section. The study of the Pedrógão Grande-Góis event focuses on the second day of the event (June 18, 2017) because no satellite measurements are available at the starting day due to the presence of clouds and thick smoke. The event took place within a context of extreme high temperatures, with values of up to 40ºC registered at the station nearest to the affected region, and relative humidity as low as 20%. Besides killing 64 people, the fire involved more than 1 000 fire fighters, destroyed almost 500 buildings and a continuous patch of more than 42 000 ha burned in one week. In the case of the fire episodes near Marseille, two large fires that started on July 24, 2017 and burned more than 3 000 ha are analyzed, the study focusing on the day after the onset because of the recorded high values of released energy during that day. As mentioned in the Introduction several other episodes occurred in the area during that week, more than 2 000 fire fighters were deployed and more than 10 000 people had to be evacuated.

4 Results

4.1 General features of energy released by fires

Figure 4 shows the monthly median values of daily energy released by fires at each pixel. The distributions represent the whole calibration period (2010 – 2016), and reveal an absolute maximum of 110 GJ in August and an absolute minimum of 42 GJ in May, closely followed by a local minimum of 49 GJ in November. All monthly distributions are positively skewed and the annual cycle of interquartile range presents a very similar behavior to that of the median, with the monthly values of the former presenting an absolute maximum of 333 GJ in August and an absolute minimum of 78 GJ in November, followed by a local minimum of 91 GJ in May. This behavior is to be expected since fire events with low values of released energy are less conditioned by meteorological factors and are therefore likely to occur all over the year whereas fire events releasing high values of energy depend on favorable weather conditions that are more frequent in the summer months. It is also worth noting that monthly values of the median for the validation period (January–August 2017) are larger than the corresponding values for the calibration period in all months but May thus stressing the fire-prone year of 2017.

Nat. Hazards Earth Syst. Sci. Discuss., https://doi.org/10.5194/nhess-2017-346
Manuscript under review for journal Nat. Hazards Earth Syst. Sci.
Discussion started: 13 October 2017

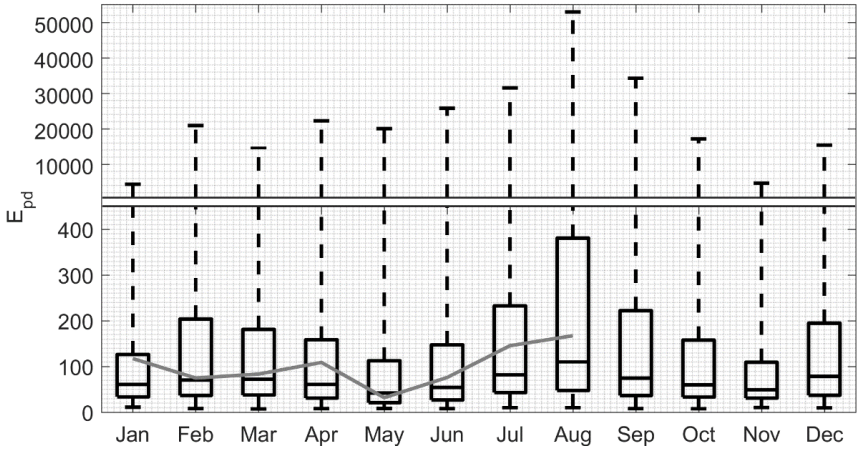

Figure 4: Monthly distributions of daily energy (GJ) released per pixel during the calibration period (2010–2016). Monthly values of the median are indicated by the horizontal line inside each box, the first and third quartiles are indicated by the bottom and top sides of the box and the maximum and minimum values by the whiskers. The superimposed grey curve shows the values of the monthly medians during the validation period (January–August 2017).

The spatial distribution of energy released by wildfires was analyzed by adding up for every pixel in the study area the daily values of released energy recorded during the calibration period (2010–2016). As shown in Fig. 5, a large patch of high values of total released energy may be identified over the northwest of the Iberian Peninsula with the highest values located in the forested lands of Central Portugal. An elongated patch of high values may be also identified along the Mediterranean coast of Africa, the highest values occurring in the forested areas of Morocco, Algeria and northern Tunisia. Other patches albeit reaching less high values of total released energy may be identified in Central Europe, in Bulgaria and Romania, in Southern Italy as well as in Sicily and Sardinia.

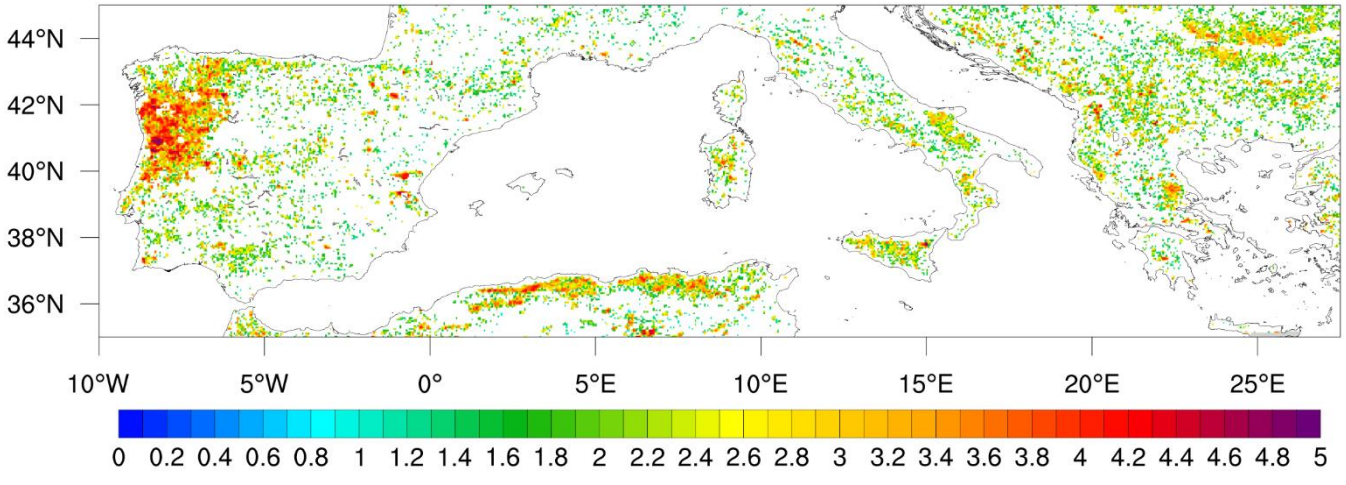

Figure 5: Geographical distribution of total energy released by fire recorded during the calibration period (2010–2016). The colour bar indicates the values of the decimal logarithm of the total energy ($\log_{10}$ E, with E in GJ).

Nat. Hazards Earth Syst. Sci. Discuss., https://doi.org/10.5194/nhess-2017-346
Manuscript under review for journal Nat. Hazards Earth Syst. Sci.
Discussion started: 13 October 2017

Natural Hazards and Earth System Sciences Discussions

The distributions of daily released energy per pixel for the three considered types of vegetation cover/land use (Fig. 6) show that pixels covered by forests have the largest values of both the median and the interquartile range, followed by shrubland and cultivated areas. These results are in agreement with the findings by Moreira et al. (2011), Fernandes (2013) and DaCamara et al. (2014) pointing out that within the Mediterranean basin long-lasting and intense fire episodes are more frequent in forests and shrubland than in cultivated areas.

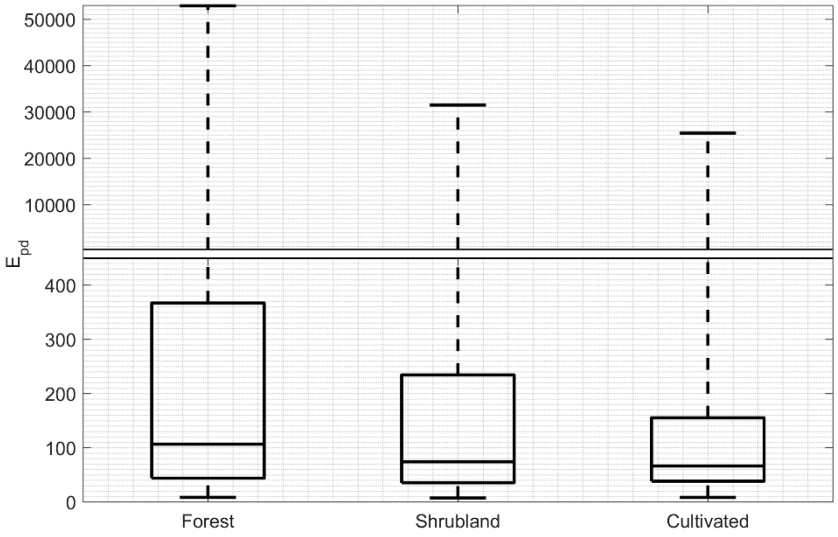

Figure 6: As in Fig. 4 but for the distribution of daily energy (GJ) released per pixel stratified by type of vegetation cover/ land use.

4.2 Statistical models of exceedance of energy released by fires

Probability of exceedance of daily energy per pixel released by fires was computed over the study area according to the procedure described in Sect. 3.3. Statistical models of exceedance were then built as described in Sect. 3.4, starting by adjusting a GP model to the sample of daily values of energy exceeding a prescribed threshold (null model) and then improving the null model by using static probability and FWI anomaly as covariates of the scale parameter (Daily Model). In order to reduce false alarms, the computation of daily energy per pixel (which characterizes each fire event) was restricted to days where the maximum value of confidence of FRP was at least 99%.

4.2.1 Static probability

Values of static probability were computed over the study area for 20 thresholds ranging from 100 up to 2000 GJ with steps of 100 GJ. The geographical distribution of values of probability of exceedance for the threshold of 2000 GJ and the respective distributions by type of vegetation cover/land use are shown in Fig. 7 and in Fig. 8, respectively. Most spatial discontinuities in the field of $P(2000|0)$ reflect changes in vegetation cover (Fig. 1) but there are some areas, e.g. in North Africa, that

Nat. Hazards Earth Syst. Sci. Discuss., https://doi.org/10.5194/nhess-2017-346
Manuscript under review for journal Nat. Hazards Earth Syst. Sci.
Discussion started: 13 October 2017

Natural Hazards and Earth System Sciences
Discussions

although belonging to the same type of vegetation cover/land use present changes in static probability which are associated to the spatial variability of the energy released by recorded fire events (Fig. 5).

Regarding the distribution of $P(2000|0)$ for the three considered types of vegetation cover/land use (Fig. 8), it is seen that, as expected, there is a close agreement between the distributions of static probability of exceedance and that of daily released energy per pixel (Fig. 6). Again, $P(2000|0)$ shows a clear distinction among the three types of vegetation, forests with the highest values of the three quartiles and cultivated areas with the lowest.

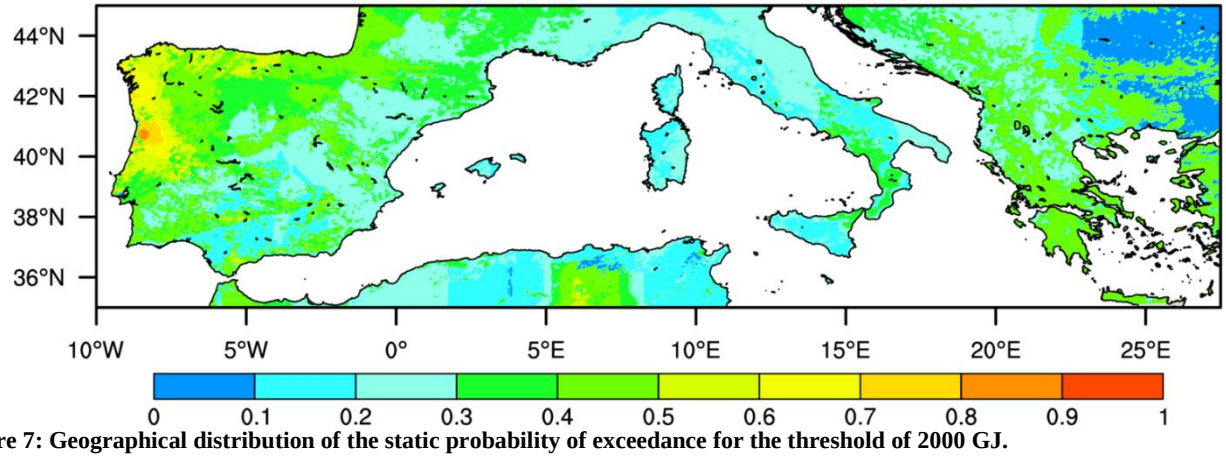

Figure 7: Geographical distribution of the static probability of exceedance for the threshold of 2000 GJ.

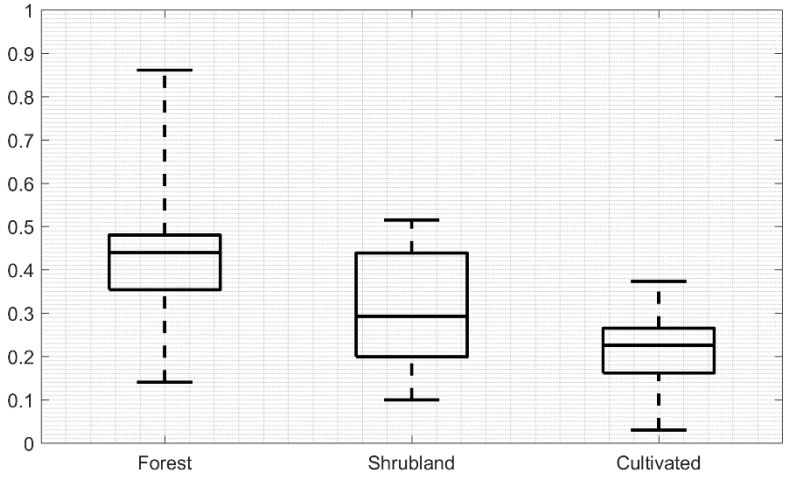

Figure 8: As in Fig. 6 but for the distribution of static probability of exceedance of the threshold of 2000 GJ.

Nat. Hazards Earth Syst. Sci. Discuss., https://doi.org/10.5194/nhess-2017-346
Manuscript under review for journal Nat. Hazards Earth Syst. Sci.
Discussion started: 13 October 2017

Natural Hazards and Earth System Sciences Discussions

4.2.2 Null model

As described in Sect. 3.4, the choice of E_{min} threshold to be used in the GP distributions of daily released energy per pixel was based on the visual inspection of a plot of the sample mean of the values exceeding successive thresholds as a function of the respective threshold. Tested values of thresholds ranged from 0 to 1000 GJ with steps of 100 GJ. The chosen value $E_{min} = 200$ GJ is such that above that value the dependence of exceeding means on thresholds becomes linear. The size of the sample obtained using this threshold is 5630, representing 93% of the original sample of recorded daily values of energy per pixel. Maximum likelihood estimates of the shape (α) and scale (σ) parameters of the GP distribution exceedances of energy (over 200 J) lead to the values of $\alpha = 0.30$ and $\sigma = 1719$ with corresponding 95% confidence intervals of $[0.26, 0.33]$ and $[1647, 1794]$, respectively. Using the Anderson-Darling test, the null hypothesis that the sample of exceedances are drawn from a GP distribution was accepted at the 42% significance level, (i.e. the probability of rejecting the null hypothesis given that it is true is 42%). The goodness of fit was also visually confirmed by plotting sample quantiles against GP quantiles (Fig. 9). For values of exceedance greater than 2×10^4 GJ a progressive departure from the 1:1 line is observed in the quantile-quantile plot, however, these values represent only 0.6% of the sample size and are likely due to the saturation of the SEVIRI sensor that occurs at about 1000 MW per pixel (Wooster et al., 2005).

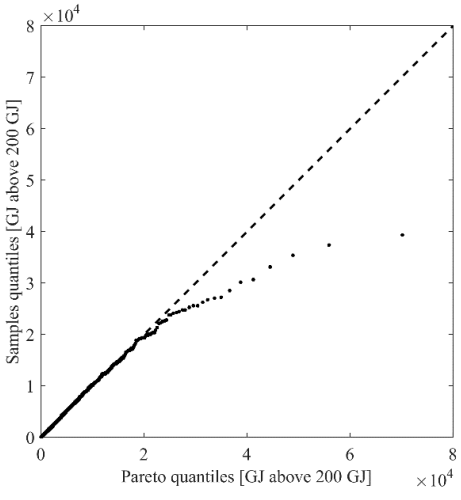

Figure 9: Quantile-quantile plot for the fitted GP distribution. The dashed segment represents the 1:1 line.

4.2.3 Daily Model

Occurrence of large fires releasing large amounts of energy is expected to be more frequent in regions with high values of static probability. Large events are also likely to be steered by meteorological conditions favouring the ignition and propagation of fire, i.e. associated to large positive values of FWI anomalies. This is shown in Fig. 10, where the daily energy per pixel

Nat. Hazards Earth Syst. Sci. Discuss., https://doi.org/10.5194/nhess-2017-346
Manuscript under review for journal Nat. Hazards Earth Syst. Sci.
Discussion started: 13 October 2017

released by recorded fire events during 2010–2016 is plotted as a function of FWI^* and $P(2000|0)$. As expected, events releasing very high values of energy are mostly preferably associated to high positive values of FWI^* and/or $P(2000|0)$.

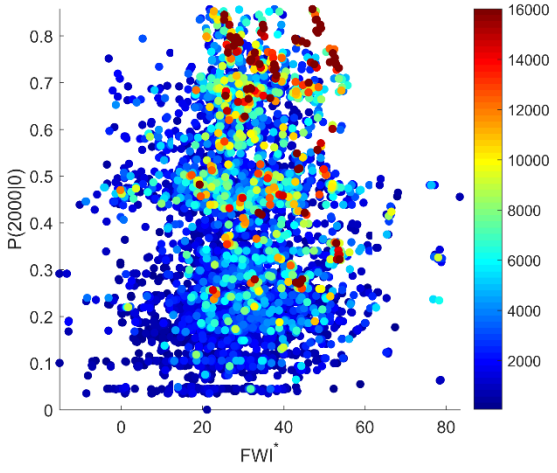

Figure 10: Daily energy per pixel released by fires as a function of FWI^* and $P(2000|0)$. Circles are coloured according to the released energy (GJ).

These results suggest improving the performance of the null model by incorporating FWI^* and $P(2000|0)$ as covariates of the scale (σ) parameter of the GP distribution. Using a procedure similar to the one proposed by DaCamara et al. (2014), the dataset of energy exceedances was stratified into 51×51 cells by scrolling the domain $FWI^* \times P(2000|0)$ by a sliding window successively defined by values of FWI^* and $P(2000|0)$ ranging between corresponding minimum and 50th percentile, 1st and 51st percentiles, and so on up to between 51st percentile and the maximum with steps of 1%, leading to a total amount of 2601 cells. Each cell was characterized by the respective mean values of FWI^* and $P(2000|0)$ of its sides. GP distributions were then adjusted to each cell and estimated values of the scale parameter (σ) were assigned to the respective cell. The two following boundary conditions were also defined in the domain translating the fact that no fires are expected at the lower bounds of both FWI^* and $P(2000|0)$: $\sigma \equiv 1$ along FWI* = -15 (the minimum value observed) and along $P(2000|0)$= 0.

The behaviour of σ as a function of FWI^* and $P(2000|0)$ was then modelled by means of a feed forward artificial neural network with one hidden layer with 3 neurons and the sigmoid function for activation (Haykin, 2009). The number of neurons was set by subdividing the data into a training set and a test set, and successfully trying different number of neurons so that both underfitting and overfitting of the model to the dataset is avoided. The results are shown in Fig. 11 and, as expected, σ monotonically increases with covariates FWI^* and $P(2000|0)$. It may be also noted that the larger the values of the covariates the closer is σ to a linear dependence.

Nat. Hazards Earth Syst. Sci. Discuss., https://doi.org/10.5194/nhess-2017-346
Manuscript under review for journal Nat. Hazards Earth Syst. Sci.
Discussion started: 13 October 2017

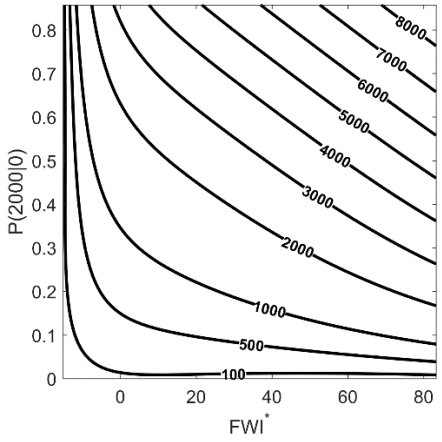

Figure 11: Dependence of scale parameter σ of the GP distribution on covariates FWI* and P(2000|0) as modelled by the neural network.

A new model (Daily Model) was then set up by replacing the constant scale parameter of the null model by a spatially and temporally variable one, as determined by covariates FWI^* and $P(2000|0)$. The null hypothesis of similar performance of both null and Daily Models was rejected by the likelihood ratio test given that the obtained p-value was lower than 0.0001. Goodness of fit of the Daily Model was then visually assessed by comparing probabilities $P(2000|200)$ computed with the Daily Model using Eq. (5) against empirical probabilities estimated from observations. For this purpose, the dataset of daily values of $P(2000|200)$ over the study area during the calibration period was stratified into intervals of probability by means of a sliding window of probability successively ranging from 0 to 0.2, 0.05 to 0.25, and so on up to from 0.8 to 1, with a range of 0.2 and increments of 0.05. At each step, fire events in pixels associated to selected probabilities were counted, namely the numbers N_{200} and N_{2000} of fires occurrences with energy release above 200 and 2000 GJ. In order to have sufficiently large samples, retained steps were restricted to those containing more than 200 fire events releasing more than 200 GJ (i.e. $N_{200} > 200$). The empirical probability of each step was accordingly computed as the ratio N_{2000}/N_{200} and this value compared to the mid-range of $P(2000|200)$ associated to the sliding window at that step. As shown in Fig. 12 when empirical values of probability are plotted against respective mid-range values of $P(2000|200)$, a good fit is achieved between points and the 1:1 line.

Nat. Hazards Earth Syst. Sci. Discuss., https://doi.org/10.5194/nhess-2017-346
Manuscript under review for journal Nat. Hazards Earth Syst. Sci.
Discussion started: 13 October 2017

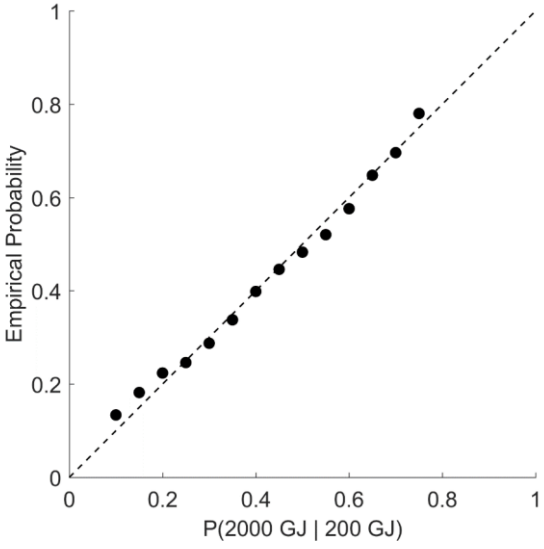

Figure 12: Empirical values of probability computed from observations of fire events as a function of $P(2000|200)$ derived from the Daily Model during the calibration period (2010–2016).

4.3 Classes of fire danger and model performance

Classes of fire danger were defined following the procedure described in Sect. 3.5, i.e. by plotting, for the whole study area during the calibration period, each value of daily energy E_{pd} released in day d at pixel p (Fig. 13). As expected, there is an increase in occurrence of higher values of released energy with increasing probability of exceedance G and anomaly A. The horizontal line γ_0 separates the "Low" class from the remaining ones. This class contains 436 events that represent only 7% of the total amount of 6050 events. The remaining classes are delimited by curves, $(\gamma_1, \gamma_2, \gamma_3)$ defined by break points $(P_1, P_2, P_3) = (0.095, 0.190, 0.285)$. As prescribed in the procedure, break points are equally spaced by 0.095 and the "Very High" and "Extreme" classes contain about the same number of events, i.e. 1780 and 1830, representing 29 and 30 % of the total amount, respectively.

A better insight into the characteristics of the Daily Model's five classes of danger may be obtained by stratifying the occurrences into three ranges of energy released by the fire events, namely below 2000 GJ, between 2000 and 10 000 GJ and above 10 000 GJ. As shown in Table 1 ('Daily Model' sub-table), within the cases of the lowest range (< 2000 GJ), 57 % are almost equally distributed between the "High" (29 %) and "Very High" (28 %) classes, while the intermediate range (2000–10 000 GJ) presents a steep increase in frequency from "Low" to "Extreme". An even steeper increase is observed for the upper range (> 10 000 GJ), for which the "Low" and "Moderate" classes contain no cases and the "Extreme" one concentrating 79% of the events in that layer.

Nat. Hazards Earth Syst. Sci. Discuss., https://doi.org/10.5194/nhess-2017-346
Manuscript under review for journal Nat. Hazards Earth Syst. Sci.
Discussion started: 13 October 2017

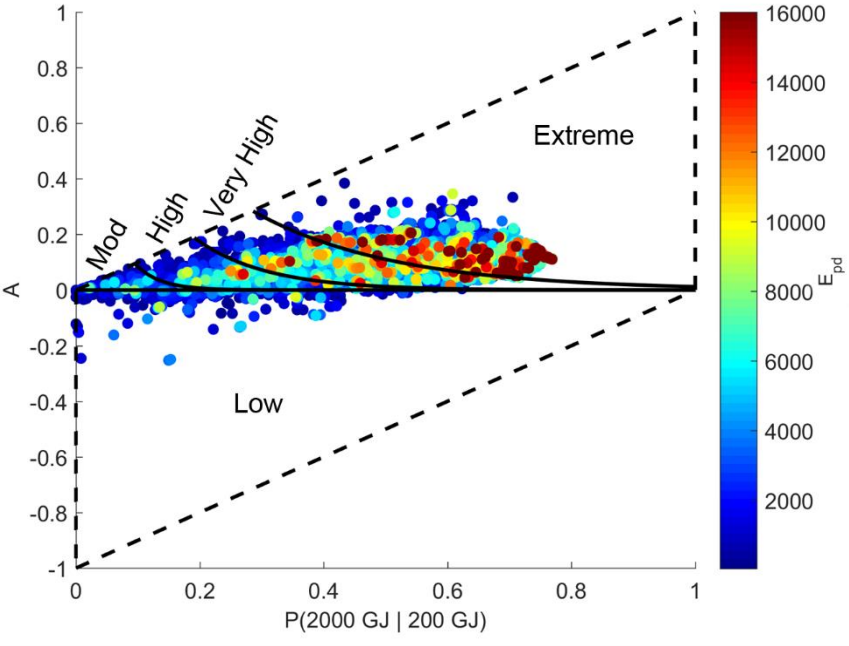

Figure 13: As in Fig. 3 but respecting to results for the calibration period (2010–2016) based on values of $P(2000|200)$ and respective anomalies A. Fire events during the period are superimposed, being represented by circles coloured according to the daily released energy (GJ).

Table 1: Distributions during the calibration period (2010–2016) of fire events among classes of fire danger for three ranges of daily energy released by fires when classes are obtained from the Daily Model, the LSA SAF product and the EFFIS module. Each cell contains the number of observed events and [in brackets] the corresponding fraction (%) of the total number of events belonging to the same energy layer.

	Energy [GJ]	Low	Moderate	High	Very High	Extreme	Total
Daily Model	< 2000	367 [10]	531 [14]	1102 [29]	1070 [28]	714 [19]	3784 [100]
	2000–10000	69 [3]	52 [3]	315 [15]	669 [33]	948 [46]	2053 [100]
	> 10000	0 [0]	0 [0]	4 [2]	41 [19]	168 [79]	213 [100]
LSA-SAF	< 2000	98 [3]	219 [6]	1417 [37]	1513 [40]	537 [14]	3784 [100]
	2000–10000	19 [1]	53 [3]	475 [23]	1080 [52]	426 [21]	2053 [100]
	> 10000	0 [0]	0 [0]	14 [7]	119 [56]	80 [37]	213 [100]
EFFIS	< 2000	101 [3]	181 [5]	1248 [33]	1419 [37]	835 [22]	3784 [100]
	2000–10000	32 [2]	66 [3]	720 [35]	708 [34]	527 [26]	2053 [100]
	> 10000	1 [1]	2 [1]	58 [27]	70 [33]	82 [38]	213 [100]

As mentioned in Sect. 3.6, the performance of the Daily Model is assessed by comparing the distributions of events among the classes of fire danger for the three ranges of energy with those obtained when using the LSA SAF and the EFFIS products

(Table 1, 'LSA SAF´and 'EFFIS' subtables). Differences are particularly notable in the upper energy range (>10 000 GJ), especially for EFFIS classes where events spread in all classes and the "Very High" and "Extreme" classes only contain 71% of the cases whereas for the Daily Model and the LSA SAF they contain 98 and 93 %, respectively. However in the case of LSA SAF classes, the modal class is the "Very High" and not the "Extreme" as in the Daily Model. Similar differences, although less prominent, may be observed among the three products in the intermediate energy range (2000–10 000 GJ). The modal classes are the "Extreme", the "Very High" and the "High" for the Daily Model, the LSA SAF and EFFIS respectively, with the modal frequency being the highest (52 %) for the LSA SAF, followed by the Daily Model (46 %) and EFFIS where the value (35 %) is quite low and very close to the value of the class immediately above (34 %). Finally, the lower energy range (< 2000 GJ) also presents differences among the three products, namely in the frequency of events in the "Low" and "Moderate" classes, that represent 24 % of the events in the Daily Model and only 9 and 8 % for the LSA SAF and EFFIS.

The different features of the classes from the three products ultimately translate into different values of probability of a fire event releasing a given amount of energy in case of a given class danger. For instance, using results presented in Table 1, the conditional probability of having a large release of energy (> 10 000 GJ) given "Extreme" danger is 168/1830 = 9.1 %, 80/1043 = 7.7 % and 82/1444 = 5.7 %, respectively for the Daily Model, the LSA SAF and EFFIS, whereas the conditional probability of having a small release of energy (< 2000 GJ) given "Low" danger is 367/436 = 84.2 %, 98/117 = 83.8% and 101/134 = 75.4 %. Differences among values of probability obtained for the three products in these two situations point out the better performance of the Daily Model if the aim is to have information about the probability of occurrence of an event releasing a given amount of energy. This result is not surprising since the Daily Model was specifically designed for such purpose. Estimates of probability by the LSA SAF product are closer to those by the Daily Model than the ones by EFFIS because the LSA SAF relies on duration of active fires inside each pixel and day that is a better proxy of energy released by fires than records of fire events with more than 500 ha of burned area. We nevertheless acknowledge that it is not a straightforward exercise to translate the 6 danger classes defined by EFFIS into a 5 class scheme such as those of the LSA SAF and Daily Model approaches.

4.4 Model validation

As described in Sect. 3.6, model validation involves applying the Daily Model to the validation period (January–August 2017) and analysing results obtained for the two severe events of Pedrógão Grande-Góis (Portugal) and Provence (France). It is important to note that, contrasting to the calibration period where meteorological data were obtained from ERA-Interim reanalysis, ECMWF's operational 24-hour forecasts are used during the validation period. The overall coherence of reanalysis data makes them especially appropriate to calibrate the Daily Model but forecast information has to be used for operational application. Results obtained in the validation period therefore reflect the effects of applying the procedure to an independent dataset as well as those due to using forecast information instead of reanalyses.

As shown in Table 2, during the validation period, the obtained distributions of events among classes of fire danger are similar to those obtained in the calibration (Table 1, 'Daily Model' subtable). The distribution of events for the lowest range (< 2000

GJ) is slightly shifted toward the more severe classes of fire danger, the modal class being the "Very High" one, with almost half (49 %) of the events and the "Extreme" class containing 20 % of the cases, a figure very close to the one obtained in the calibration period (19 %). The intermediate range (2000–10 000 GJ) is slightly shifted towards the lower classes of fire danger, the modal class (like in the lowest range) being the "Very High" with 49 % of the events, but, like in calibration, the highest jump in relative frequency is from the "High" to the "Very High" class (13 to 49 %). In the highest range (>10 000 GJ), like in calibration, no cases are observed in the "Low" and "Moderate" classes, virtually all cases (all but one) belonging to the "Very High" and "Extreme" classes, although a smaller fraction (66 %) than in calibration (79%) is contained by the "Extreme" class.

The conditional probability of having a large release of energy (> 10 000 GJ) given "Extreme" danger is 97/583 = 17.2 %, almost the double than in calibration (9.1 %), a feature that may be attributed to the fact that up to August, according to information at the EFFIS site, the cumulated burned area in 2017 is more than 500 000 ha, two and half times the 2008–2016 average of about 200 000 ha. This may also explain the virtual absence of episodes in the "Low" class (4 events in a total of 1851).

Table 2: As in Table 1 but for distributions obtained in the validation period (January–August 2017) of fire events among classes of fire danger as obtained from the Daily Model.

	Energy [GJ]	Low	Moderate	High	Very High	Extreme	Total
Daily Model	< 2000	1 [0]	54 [6]	239 [25]	460 [49]	183 [20]	937 [100]
	2000–10000	3 [0]	5 [1]	103 [13]	374 [49]	283 [37]	768 [100]
	> 10000	0 [0]	0 [0]	1 [1]	48 [33]	97 [66]	146 [100]

Results for the severe event at Pedrógão Grande-Góis (Portugal) are shown in Fig. 14 (left panel). It is worth noting that on June 18, 2017 the area surrounding the fire events is covered by a patch of values of $P(2000|200)$ exceeding 0.5 (top frame) over a background of lower values covering most of the Mediterranean basin. Pixels inside the area of interest (black boxes) are mostly classified as "Extreme" danger of fire (lower left frame) and active fires detected (reaching up to 5000 GJ of released energy) are within or very close to the border of the partition classified as "Extreme" fire danger in the domain of $P(2000|200)$ versus anomaly A (lower right frame). The fire episodes near Marseille Fig. 14 (right panel) took place within an area conspicuously characterized by values of anomalies A above 0.3, which are higher than the surrounding values and much higher that the values observed in the vast majority of pixels over the Mediterranean basin. The fire events near Marseille (reaching up to 10 000 GJ of released energy) are located within the area classified as "Extreme" danger of fire (lower left frame) and, as those of Pedrógão Grande-Góis occurred within the most severe class or near the border between "Extreme" and "Very High" fire danger. There is however a difference between those two events that is worth mentioning. In the case of Pedrógão Grande-Góis, pixels where active fires were observed are classified as or near "Extreme" fire danger because of the high values of $P(2000|200)$, whereas in the case of Provence it is mostly because of the high values of anomaly A. The two

Nat. Hazards Earth Syst. Sci. Discuss., https://doi.org/10.5194/nhess-2017-346
Manuscript under review for journal Nat. Hazards Earth Syst. Sci.
Discussion started: 13 October 2017

Natural Hazards and Earth System Sciences
Discussions

cases are therefore a good example that justifies the rationale of defining the classes of fire danger in the space $P(2000|200)$ versus anomalies A.

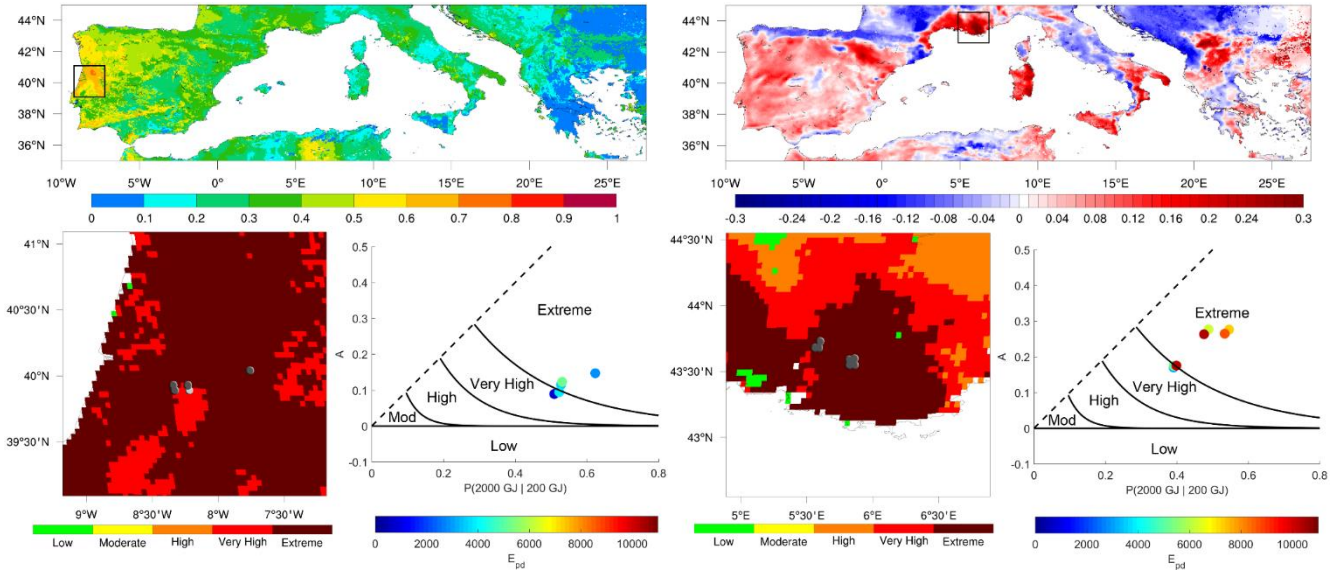

Figure 14: Results obtained for the 2017 fire events at Pedrógão Grande-Góis (Portugal) on June 18 (left panel) and near Marseille (France) on July 25 (right panel). The geographical distributions over the Mediterranean basin of P(2000|200) for Pedrógão Grande-Góis and of anomaly *A* for Provence are shown in the upper frames of the respective panels and the areas of interest are represented by the two corresponding black boxes. Classes of fire danger for the areas of interest are shown in the colorbar of the lower left frames, together with the observed active fire events (dark grey circles). Locations of fire events (colored circles) in the space of P(2000|200) versus anomaly *A* are shown in the lower right frames, the colors indicating the amount of the daily released energy E_{pd} (in GJ).

5 Conclusions

The Mediterranean is one of the regions of the world most affected by large wildfires and fire prevention is therefore of crucial importance. Fire prevention requires adequate knowledge about wildfire potential assessment that is usually based on fire danger rating systems providing indices to be used on an operational and tactical basis in wildfire management decision support systems.

The aim of the present work is to lay the grounds towards the development of an operational product that will be able to provide the user community with daily information on meteorological danger that will allow adopting the adequate measures to mitigate fire damage. The proposed product consists of forecasts of fire danger over Mediterranean Europe based on a statistical procedure that combines information about fire history derived from the Fire Radiative Power (FRP) product by the Satellite Application Facility for Land Surface Analysis (LSA SAF) with daily meteorological forecasts provided by the European Centre for Medium-Range Weather Forecasts (ECMWF).

The procedure involves estimating static and daily probabilities of exceedance of daily energy released by fires occurring at the pixel level. Static probability at a given pixel is estimated by the ratio of the number of daily fire occurrences releasing energy above a given threshold to the total number of occurrences inside a cell centered at the point. Daily probability takes into account meteorological factors by means of the Canadian Fire Weather Index (FWI) and is estimated using a Daily Model based on a Generalized Pareto distribution with static probability and FWI as covariates of the scale parameter. Five classes of fire danger are then associated to daily probability estimated by the Daily Model.

During the calibration period (2010–2016), it is shown that when using the Daily Model 79 % of fire events releasing daily energy above 10 000 GJ are contained in the "Extreme" class of fire danger and that this number reduces to 37 % (38 %) when the classes are from the currently operational LSA SAF (EFFIS) product. It is also shown that the "Low" class from the Daily Model contains 10 % of events with released daily energy lower than 2000 GJ, whereas this percentage is only 3 % when classes from LSA SAF or EFFIS are used. Classes of fire danger from the Daily Model are therefore more able to discriminate fire events in terms of released energy. This becomes clear when comparing results of conditional probabilities of having a large (small) release of energy given "Extreme" ("Low") danger. For instance, the probability of released energy greater than 10 000 GJ given the "Extreme" class of fire danger is 9.1 %, 7.7 % and 5.7 % when using the Daily Model, LSA SAF and EFFIS, whereas the probability of released energy lower than 2000 GJ given the Low class is 84.2 %, 83.8 % and 75.4 %, respectively. When the Daily Model is applied to the independent dataset of January–August 2017, results are consistent with those obtained in calibration.

The product derived from the proposed Daily Model mainly differs from LSA SAF and EFFIS products in that the indices of meteorological fire danger are calibrated based on seven years of information about fire radiative power, with a temporal resolution of 15 minutes as derived from the SEVIRI instrument on-board MSG satellites. Besides providing a solid physical meaning to the approach since energy is a measurable physical property, fire radiative power is also directly related to the amount of fuel burned and smoke production (e.g. Wooster et al., 2005). Fire radiative power is also useful in fire management and firefighting because it can be used as a proxy of fire line intensity (Smith and Wooster, 2005). Insofar as fire radiative power is derived from remote-sensed information by the same instrument, observations are consistently performed in space and time, an advantage over the traditional approaches where the calibration procedures are performed by means of analyses of fire weather history based on ground observations of amount of burned area or on the number of fire occurrences that are affected by the policy of individual countries and by changes in criteria along time (Pereira et al., 2011).

A prototype of the proposed procedure is running since April 2017 at Instituto Dom Luiz, Faculty of Sciences, University of Lisbon (http://idlcc.fc.ul.pt/CeaseFire/). Besides assisting in wildfire management, information provided about the statistical distributions of exceedances in fire radiative power, as well as of meteorological parameters and derived indices of fire danger is expected to represent an added value in decision making on prescribed burning within the framework of agricultural and forest management practices, a very delicate activity since wrong or uninformed decisions may trigger severe events associated to large damages.

References

Amraoui, M., Liberato M. L. R., Calado, T. J., DaCamara, C. C., Pinto-Coelho, L., Trigo, R. M. and Gouveia, C. M.: Fire activity over Mediterranean Europe based on information from Meteosat-8, Forest Ecol. Manag., 294, 62–75, doi: 10.1016/j.foreco.2012.08.032, 2013.

Amraoui, M., Pereira, M. G., DaCamara, C. C. and Calado, T. J.: Atmospheric conditions associated with extreme fire activity in the Western Mediterranean region, Sci. Total Environ., 524–525, 32–39, doi: 10.1016/j.scitotenv.2015.04.032, 2015.

Anderson, T. W. and Darling D. A.: Asymptotic Theory of Certain "Goodness of Fit" Criteria Based on Stochastic Processes. Annals of Mathematical Statistics, 23, 193–212. doi:10.1214/aoms/1177729437, 1952.

Coles, S.: An Introduction to Statistical Modeling of Extreme Values, 208 pp., Springer, London, 2001.

DaCamara, C. C., Calado, T. J., Ermida, S. L., Trigo, I. F., Amraoui, M. and Turkman, K. F.: Calibration of the Fire Weather Index over Mediterranean Europe based on fire activity retrieved from MSG satellite imagery, Int. J. Wildland Fire, 23, 945–958, doi: 10.1071/WF13157, 2014

de Zea Bermudez, P., Kotz, S.: Parameter estimation of the generalized Pareto distribution - Part II, J. Stat. Plan. Inference, 140, 1374-1388. doi:10.1016/j.jspi.2008.11.020, 2010.

Dee, D. P., Uppala, S. M., Simmons, A. J., Berrisford, P., Poli, P., Kobayashi, S., Andrae, U., Balmaseda, M. A., Balsamo, G., Bauer, P., Bechtold, P., Beljaars, A. C. M., van de Berg, L., Bidlot, J., Bormann, N., Delson, C., Dragani, R., Fuentes, M., Geer, A. J., Haimberger, L., Healy, S. B., Hersbach, H., Hólm, E. V., Isaksen, L., Kallberg, P., Köhler, M., Matricardi, M., McNally, A. P., Monge-Sanz, B. M., Morcrette, J-J., Park, B-K., Peubey, C., de Rosnay, P., Tavolato, C., Thépaut, J-N., Vitart, F.: The ERA-Interim reanalysis: Configuration and performance of the data assimilation system, Q. J. R. Meteorol. Soc., 137(656), 553–597, doi: 10.1002/qj.828, 2011.

EUMETSAT: LRIT/HRIT Global Specification, EUMETSAT, Coordination group for meteorological satellites, CGMS03, Darmstadt, Germany, 1999.

Fernandes, P. M.: Fire-smart management of forest landscapes in the Mediterranean basin under global change. Landsc. Urban Plan., 110, 175–182, doi:10.1016/J.LANDURBPLAN.2012.10.014, 2013.

Finney, M. A.: The challenge of quantitative risk analysis for wildland fire, Forest Ecol. Manag., 211, 97–108, doi: 10.1016/j.foreco.2005.02.010, 2005.

Grimshaw, S. D.: Computing Maximum Likelihood Estimates for the Generalized Pareto Distribution. Technometrics, 35, 185-191. doi:10.2307/1269663, 1993.

Hagan, M. T. and Menhaj, M.: Training feed-forward networks with the Marquardt algorithm. IEEE Transactions on Neural Networks, 5, 989-993, 1994.

Haiden, T., Janousek, M., Bidlot, J., Ferranti, L., Prates, F., Vitart, F., Bauer, P. and Richardson D.S.: Evaluation of ECMWF forecasts, including the 2016 resolution upgrade, Technical Memorandum 792, European Centre for Medium-Range Weather Forecasts, Reading, Berkshire, 55 pp., 2016.

Hartley, A., Pekel, J-F., Ledwith, M., Champeaux, J-L., De Badts, E. and Bartalev, S. A.: The Land Cover Map for Europe in the Year 2000, GLC2000 database, European Commission Joint Research Centre, 2006.

Haykin, S.: Neural Networks and Learning Machines, 3rd ed., Pearson, Ontario, Canada, 2009.

Lawrence, M. G.: The Relationship between Relative Humidity and the Dewpoint Temperature in Moist Air, A simple Conversion and Applications, Bull. Am. Meteorol. Soc., 86, 225–233. doi:10.1175/BAMS-86-2-225, 2005.

LSA SAF: Fire Radiative Power, Validation Report, LSA SAF, Lisbon, Portugal, 2015.

Moreira, F., Viedma, O., Arianoutsou, M., Curt, T., Koutsias, N., Rigolot, E., Barbati, A., Corona, P., Vaz, P., Xanthopoulos, G., Mouillot, F., Bilgili, E.: Landscape–wildfire interactions in Southern Europe: implications for landscape management, J. Environ. Manage., 92, 2389–2402. doi:10.1016/J.JENVMAN.2011.06.028, 2011.

Neyman, J., Pearson, E. S.: On the Problem of the Most Efficient Tests of Statistical Hypotheses, Philos. Trans. R. Soc. of Lond. A, 231, 289-337, doi:10.1098/rsta.1933.0009, 1933.

Pereira, M. G., Malamud, B. D., Trigo, R. M., and Alves, P. I.: The history and characteristics of the 1980–2005 Portuguese rural fire database, Nat. Hazards Earth Syst. Sci., 11, 3343-3358, https://doi.org/10.5194/nhess-11-3343-2011, 2011.

Pereira, M. G., Calado, T. J., DaCamara, C. C. and Calheiros, T.: Effects of regional climate change on rural fires in Portugal, Climate Res., 57, 187–200, doi: 10.3354/cr01176, 20, 2013.

Pickands, J.: Statistical inference using extreme order statistics, The Annals of Statistics, 3, 119-131, doi:10.1214/aos/1176343003, 1975.

Pyne, S. J.: Eternal Flame: An Introduction to the Fire History of the Mediterranean, in: Earth Observations of Wildland Fires in Mediterranean Ecosystems, Chuvieco, E. (Ed.), Springer-Verlag, Berlin Heidelberg, Germany, 11–26, doi:10.1007/978-3-642-01754-4, 2009.

Requardt, A., Schuck, A. and Köhl, M.: Means of combating forest dieback – EU support for maintaining forest health and vitality, iForest, 2, 38–42, doi:10.3832/ifor0480–002, 2009.

Roberts, G. J. and Wooster, M. J.: Fire Detection and Fire Characterization Over Africa Using Meteosat SEVIRI, IEEE Trans. on Geosci. and Remote Sens., 46, 1200–1218 doi: 10.1109/TGRS.2008.915751, 2008.

Ruffault J., Moron V., Trigo R. M. and Curt T.: Daily synoptic conditions associated with large fire occurrence in Mediterranean France: evidence for a wind-driven fire regime, Int. J. Climatol., 37, 524-533 doi: 10.1002/joc.4680, 2016

San-Miguel-Ayanz, J., Schulte, E., Schmuck, G., Camia, A., Strobl, P., Liberta, G., Giovando, C., Boca, R., Sedano, F., Kempeneers, P., McInerney, D., Withmore, C., Oliveira, S. S., Rodrigues, M., Durrant, T., Corti, P., Oehler, F., Vilar, L. and Amatulli, G.: Comprehensive Monitoring of Wildfires in Europe: The European Forest Fire Information System (EFFIS), Approaches to Managing Disaster – Assessing Hazards, Emergencies and Disaster Impacts, Tiefenbacher, J. (Ed.), InTech, Rijeka, Croatia, 87–108, 2012.

San-Miguel-Ayanz, J., Durrant, T., Boca, R., Libertà, G., Boccacci, F., Di Leo, M., López Pérez, J. and Schulte, E.: Forest Fires in Europe, Middle East and North Africa 2015, EUR 28158 EN, 122 pp., doi: 10.2788/914, 2016.

Smith, A. M. S. and Wooster, M. J.: Remote classification of head and backfire types from MODIS fire radiative power and smoke plume observations, Int. J. Wildland Fire, 14, 249–254, doi: 0.1071/WF05012, 2005.

Stocks, B.J., Lawson, B.D., Alexander, M.E., Van Wagner, C.E., McAlpine, R.S., Lynham, T.J. and Dube, D.E.: The Canadian Forest Fire Danger Rating System: An Overview, For. Chron., 65, 450–457, doi:10.5558/tfc65450-6, 1989.

Trigo, I. F., DaCamara, C. C., Viterbo, P., Roujean, J-L., Olesen, F., Barroso, C., Camacho-de-Coca, F., Carrer, D., Freitas, S. C., García-Haro, J., Geiger, B., Gellens-Meulenberghs, F., Ghilain, N., Meliá, J., Pessanha, L., Siljamo, N. and Arboleda, A.: The satellite application facility for land surface analysis, Int. J. Remote Sens., 32, 2725–2744, doi:10.1080/01431161003743199, 2011.

Van Wagner, C. E.: Structure of the Canadian Forest Fire Weather Index, Can. Forestry Serv., Publication 1333, Ottawa, Ont., 49 pp., 1974.

Van Wagner, C. E.: Development and structure of the Canadian Forest Fire Weather Index System, Can. Forestry Serv., Technical Report 35, Ottawa, Ontario, 48 pp., 1987.

Van Wagner, C. E. and Pickett, T. L., Equations and FORTRAN program for the Canadian forest fire weather index system, Can. Forestry Serv., Technical Report 33, Chalk River, Ontario, 18 pp., 1985.

Viegas, D. X., Bovio, G., Ferreira, A., Nosenzo, A. and Sol, B.: Comparative study of various methods of fire danger evaluation in southern Europe, Int. J. Wildland Fire, 9, 235–246, doi:10.1071/WF00015, 1999.

Wooster, M. J., Roberts, G., Perry, G. L. W., Kaufman, Y. J.: Retrieval of biomass combustion rates and totals from fire radiative power observations: FRP derivation and calibration relationships between biomass consumption and fire radiative energy release, J. Geophys. Res. Atmos., 110, doi: 10.1029/2005JD006318, 2005.

Wooster, M. J., Roberts, G., Freeborn, P. H., Xu, W., Govaerts, Y., Beeby, R., He, J., Lattanzio, A., Fisher, D., Mullen, R.: LSA SAF Meteosat FRP products-Part 1: Algorithms, product contents, and analysis, Atmospheric Chemistry and Physics. 15, 13217-13239, doi: 10.5194/acp-15-13217-2015, 2015.